Energy Efficient Data Detection with Low Complexity for an Uplink Multi-user Massive MIMO System

Mohammad Kamrul Hasan[1,*], Md. Sarwar Hosain[2,*], Tonusree Saha[2], Shayla Islam[3,*], Liton Chandra Paul[4], Satish Khatak[5], Hula Mahmoud Alkhassawneh[6], Elham Kariri[7], Eshtiak Ahmed[8], and Rosilah Hassan[1]

[1] Center for Cyber Security, Faculty of Information Science and Technology, Universiti Kebangsaan Malaysia (UKM), Malaysia, 43600 Bangi, Malaysia
[2] Department of Information and Communication Engineering, Pabna University of Science and Technology, Pabna, Bangladesh
[3] Department of Computer Science, UCSI University Malaysia, 56000 Kuala Lumpur, Malaysia
[4] Department of Electrical, Electronic and Communication Engineering, Pabna University of Science and Technology, Pabna, Bangladesh
[5] Department of ECE, The Technological Institute of Textile & Sciences, Bhiwani-127021, Haryana
[6] College of Computer Science & Engineering, University of Ha'il, Kingdom of Saudi Arabia
[7] College of computer science and engineering, prince sattam bin Abdul Aziz University, Alkharj, Saudi Arabia
[8] Faculty of Information Technology and Communication Sciences, Tampere University Tampere, Finland

Correspondence: Mohammad Kamrul Hasan (Email: hasankamrul@ieee.org). Md. Sarwar Hosain (sarwar.ice@pust.ac.bd), and Shayla Islam (shayla@ucsiuniversity.edu.my)

Abstract: The current development of the Internet of Things (IoT) network in sixth-generation (6G) communication opens up various opportunities. When IoT devices with edge platforms connect to the telecommunication network, mobility, interferences, and intelligent device capacity issues might occur. The challenge with uplink MU-MIMO systems is data detection owing to noise, frequency allocations, and dense deployment of intelligent devices. The exponential complexity of extensive wireless networks makes optimal maximum likelihood detection impossible. Using MATLAB simulation-based analysis, we suggested an iterative data detection strategy based on a coordinate descent method (CDM) to reduce computing complexity while preserving an acceptable bit error rate (BER). Linear systems demand low co-channel interference (CCI) MU-MIMO uplink communications (CCI). A superior mean square error or BER performance is achieved using Maximum ratio combining with CDM. The proposed system outperforms the Richardson Method (RM), approximation message passing (AMP), and linear minimum mean square error (LMMSE) algorithms in terms of BER and complexity.

Keywords: MU-MIMO, Co-channel interferences (CCIs), Maximum ratio combining (MRC) receiver, Signal detection scheme, Total training power, Signal-to-Noise Ratio (SNR)

List of Symbols and Abbreviations:

Table 1: List of Symbols

Symbol	Definition
P_t	Leverage transmit power
n	Noise vector
G	Lognormal shadowing and Rayleigh fading
h_{ik}	Small-scale fading factor
v_k	Large-scale fading factor
σ^2	Variance of noise
y	Received signal
A	Linear detector matrix
H	Hermitian operator
Ω_p	Average envelope power
ξ	Scaling constant

1. Introduction

Technological development is critical to remain competitive in the fast-changing world of smart mobility using wireless communications. The enabling technologies that permit widespread deployment of wireless communication are enjoying their fastest growth period in history. The dense deployment of smart mobile devices in the 5G and upcoming 6G will highly impact signal-to-noise ratio (SNR), load management, and severe mobility issues. Although MIMO is the most important feature of all current broadband systems, it has yet to be implemented on a large scale because of many reasons.

Replacing the usage of classic point-to-point MIMO by MU-MIMO antenna systems that simultaneously use single-antenna terminal provided by antenna array [1].

Advanced coding algorithms are frequently used in multi-user MIMO systems to transmit data to many users at once. But, to maintain a minimal level of inter-user interference in multi-user systems, complicated interference mitigation mechanisms must be employed [2].

The LMMSE algorithm is a commonly used suboptimal detection algorithm for multi-user uplink MIMO systems due to a favorable compromise between bit error rate (BER) performance and intricacy. The complexity of the LMMSE detector, conversely, remains considerably higher for large-scale MIMO systems. For large-scale uplink MU-MIMO systems, no difference is found. Complex detectors based on LMMSE are preferred to avoid accurate inversion of large MIMO matrix. Accordingly, different classical iterative algorithms, such as the Richardson Method (RM), further decreased the entanglement of enumerating matrix inversion [3]. The AMP and its derivatives initially created for compact discovery are used in massive MIMO data detection to minimize the complexity of data detections. The advantage of the AMP-based detector is that only matrix to vector multiplication is assigned in the name of matrix-to-matrix multiplication [4]. However, the AMP algorithm needs to compete in noise variance, and low noise variance values will seriously degrade performance. In addition, AMP-assisted detectors cannot converge when MIMO channels are spatially correlated, leading to unacceptable performance. An ancient and easy technique that is remarkably effective and flexible, the coordinate descent method (CDM) has been experiencing significantly prolonged curiosity. Data optimization, machine learning, and other areas of interest contribute to its growth.

Like MRC and MMSE, linear receivers are ultimate, just like the wide varieties of antennas on the BS expand. With plenty of BS antennas, user equipment was deployed. Therefore, in a massive MIMO system, thermal noise and fading are compensated on a small scale. This paper evaluates the maximum ratio combining (MRC) receiver for many MU-MIMO systems over a composite-fading territory. The mean square error (MSE) parameter is analyzed concerning the total training power parameter in an MRC receiver's sense. System modeling with flawless channel state information (CSI) assumptions is still a pipe dream for 6G wireless networks. Deep Learning (DL) receiver architectures with channel

estimation techniques and symbol detectors are expected to become more prevalent. However, we do not know how DL models function in real-world circumstances because so many additional impairments are found. The authors recommend developing real-world benchmark channel datasets for many wireless communication systems. These benchmark datasets enable fair DL model comparison. In parallel, researchers are increasingly constructing benchmark system models. The literature increased the number of novel DL frameworks. For this reason, new DL-based methods should be evaluated for comparison with the existing and the new data-driven methodologies [5].

The rest of the article is organized as follows: Section 2 summarizes the current finding. Section 3 highlights the contributions. Section 4 presents the massive MU-MIMO system paradigm. Section 5 discusses receiver design analysis, and the Experiment results are discussed in section 6. Finally, the article is concluded in section 7.

2. Related Works

A technique proposed by Jung-Chieh Chen et al. presents a striking dispute for uplink massive MU-MIMO systems. The receiver's data detection complexity is due to the significant enlargement within the proportions of MIMO systems [6]. The ideal highest-like detector is unreal for large wireless schemes because it bears an aggressive downside for users. In contrast, Muhammad Saad Zia et al. considered the uplink of a large-scale MU-MIMO system where multiple single-antenna stations repeatedly transfer to an associate array of many antennas. For many gainer forms, the probability density function (PDF) of the gained signal to interference and noise ratio (SINR) exhibits an approximately lognormal distribution under lognormal shadowing and Rayleigh fading [7]. This paper highlights several techniques and algorithms that pursue the advantages of MIMO and space-time coding schemes and spatial multiplexing. Bukharuba, A.et al. proposed high-efficiency and low-complexity recognition and precoding algorithms for large-scale multi-user MIMO systems. These algorithms use an exciting property; the Gram matrix positively defines symmetric MIMO on a large scale. The suggested approach outperforms the linear MMSE algorithm, which would be nearly optimal for MIMO systems with multiple users but needs statistical noise data.

Additionally, the simulation results demonstrate that the suggested technique is more efficient in computational complexity and BER performance than a recently published algorithm [8]. Uncorrelated fading is another area of study in which each user's channel covariance matrix is different. Monte Carlo simulations are used to get MMSE and MRC results. Even though MMSE is the best option for enhancing capabilities, ZF processing provides higher efficiency gains. This is due to complex MMSE calculations; however, the spread of results is relatively small [9]. Another study uses a group creation algorithm to provide dynamic sub-channel mapping, which implements sub-channel discovery in HetNet based on LTE/LTE-A. This new algorithm uses synchronous receiver RSRP, distance, SNR, HeNB for group formation, CSN, and GM selection. This function is combined with the MRaSD engine for sub-channel discovery. The detection mechanism was developed to discover sub-channels of permitted MeNB and DBTV networks. This shows that the system performs better. Also, the simulation results show improved spectrum recognition. As an allocation to improve spectrum efficiency, the CCI in HetNet based on LTE/LTEA is ultimately reduced [10]. The authors of [11] proposed a new HGBBDSACTI method that can strategically allocate subcarriers, improve performance, and improve interruption. Improved system performance can alleviate CTI problems in HetNets. The main goal of their study is to allocate unoccupied subcarriers shared between HeNodeBs. Such as HeNodeB performance, average HeNodeB user performance, and power outages. The authors of [12] used the wavelet family to analyze the characteristics of a peak-to-average power ratio (PAPR) of wavelet-based OFDM (W-OFDM). They use several wavelets from different wavelet series to find out the performance of PAPR. Daubechies, Symlets, Coiflets, Biorthogonal, and Discrete Meyer are used in WOFDM, which reduce PAPR with the help of QPSK modulation. These transformations of Haar and biorthogonal discrete cosine transform show the best improvement in the wavelet family because the PAPR reaches nearly 5 dB.

As the number of femtocell and microcell coverage users increases, data and signal transmissions are sometimes interrupted by crosstalk. This interference occurs when femtocells and macrocells operate on the same carrier frequency. A method must be implemented to maximize performance and increase the spectral efficiency of wireless networks. A dynamic spectrum allocation scheme is proposed to

correlate the BER, increasing the power maximization factor in heterogeneous networks [13]. Next, the limitations of different detection algorithms used in a massive MIMO system are presented in Table 2.

Table 2: Limitations of different detection algorithms

References	Detection Algorithm used	Limitations/Gap
[14]	AMP	✓ False convergence ✓ Requires an understanding of noise variance, as an inaccurate noise variance result impairs performance
[15]	LMMSE	✓ Gram's matrix is computed using complex multiplications ✓ High computational complexity
[16]	Richardson Method	✓ A complicated Gram matrix is required ✓ Convergence needs a high number of iterations
[17]	Neumann Series	✓ When the ratio of BS antennas to user antennas is high, it suffers a significant loss in performance ✓ In compared to Newton iteration, approximation converges slowly
[18]	Sparsity based algorithms	✓ Convergence problems in Compressive sensing would be amplified by the use of sparse constraints

The goal of the CDM approach is to split down a complex optimization task into smaller, more manageable parts. As a result of the reduction in arithmetic complexity, CDM can be implemented and scaled with ease. Faster convergence, less complexity, and improved performance benefit from its low iteration rate [19].

3. Contribution

The main contribution of this paper is as follows:

- A MRC receiver is explored and integrated with the CDM methodology.
- It is generally agreed that the CDM demonstrates higher performance and is less complicated to implement than other traditional methods. Our system provided faster convergence at the low number of iterations.
- The suggested system outputs demonstrate a better BER or MSE than the current system in simulation results. It is easy to see how energy-efficient the system is by comparing the total training power for the four MSE-related methods: LMMSE, Richardson, AMP, and CDM.

4. Massive MU-MIMO System Model

MU-MIMO systems that operate in a combined fading environment are described in this section (shown in Fig. 1). We use the Rayleigh fading model in terms of small-scale fading, whereas large-scale fading is patterned using the lognormal distribution [20].

4.1 Channel Model

Our study examines the feasibility of using BS with M antennas to uplink a massive MU-MIMO system with multiple users. The BS collects data from K users by using a single antenna on the same time-frequency channel. These transmissions are distorted by channel impairments like attenuation, delay distortion, and noise (Figure 1). Equation (1) presents the received signal for $M \times 1$ signal vector in the BS.

$$y = \sqrt{\boldsymbol{P_t G_x}} + \boldsymbol{n} \tag{1}$$

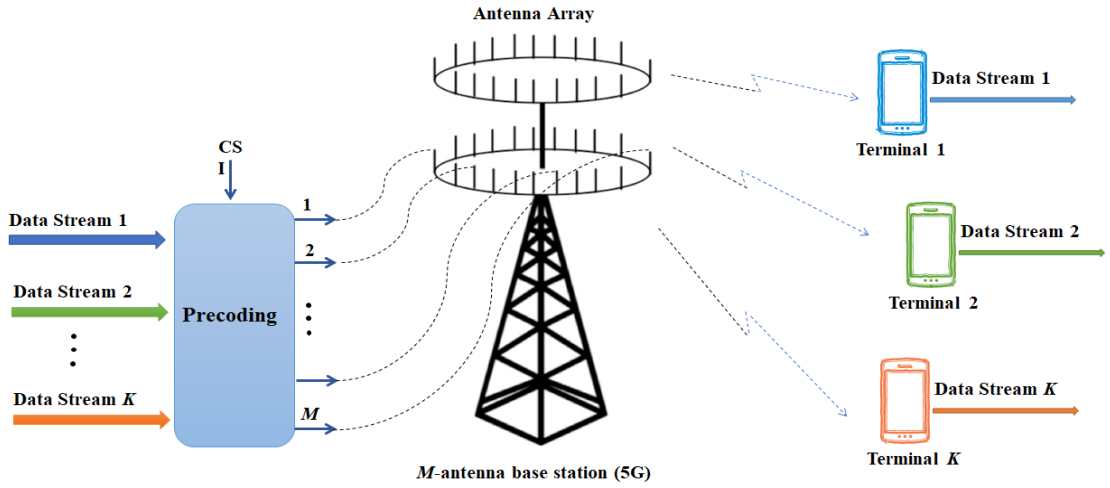

Figure 1: MU-MIMO in 5G

Between the M-antenna BS and the K users, the M x K channel matrix is indicated by G; for a single user, the average transmit power is denoted by Pt; for K concurrent users, the symbol vector x; and noise vector states by n. Rayleigh fading and lognormal shadowing are symbolized by G. Between the $\boldsymbol{k_{th}}$ users and the $\boldsymbol{i_{th}}$ BS antenna, the channel gain coefficient $\boldsymbol{g_{ik}}$ can be presented in Eqn. (2).

$$\boldsymbol{g_i} = \boldsymbol{h_{ik}}\sqrt{\boldsymbol{v_k}} \tag{2}$$

As a result, $\boldsymbol{v_k}$ offers the user's large-scale fading as $\boldsymbol{v_k} \sim \log N\ (_{(dB)}, \sigma^2)$, where $\boldsymbol{v_k}$ is the small-scale fading factor for the aforementioned antenna and users. A complex normal distribution with zero mean and unit variance $\boldsymbol{h_{ik}} \sim \mathcal{C}\mathrm{N}(0,1)$, where $\boldsymbol{h_{ik}}$ is the Rayleigh fading coefficient in a Rayleigh fading environment. BS antennas are oriented in such a way that users outside the M-antenna BS experience large-scale fading.

Although, the small-scale fading factors are unconventional and equivalently circulated. This study assumes a perfect correlation between a single user's shadowing components over M-antenna BS. Consequently, the received signals from the $\boldsymbol{k_{th}}$ user through M-antenna BS supports uniform shadowing. The channel matrix can be presented in Eqn. (3).

$$G = HV^{1/2} \tag{3}$$

Small fading coefficients between K users and the M-antenna BS are represented by H, an $M \times K$ matrix, and $K \times K$ diagonal matrix of K users is denoted by V. Next, the received signal y is refined using a linear detector as presented in Eqn. (4).

$$r = A^H y \tag{4}$$

The vector *r* symbolizes the acquired signals from all users in the equation, where *A* is the linear detection matrix. *G* and *H* represent the channel matrix and Hermitian operator, respectively.

4.2 SINR Calculation

The obtained signal vector is likely to be after putting the linear detector (r) shows Eqn. (4)

$$r = \sqrt{P_t} A^H G x + A^H n \tag{5}$$

To calculate a user's SINR, the vector *r* is divided into two components. Let x_j and r_j signify the $\boldsymbol{j_{th}}$ user's sent symbol and received signal, respectively shown in Eqn. (6).

$$\begin{aligned} \boldsymbol{r_j} &= \sqrt{\boldsymbol{P_t}}\boldsymbol{a_j^H g_j x_j} \\ &= \sqrt{\boldsymbol{P_t}} \sum\nolimits_{\boldsymbol{k=1, k\neq j}}^{\boldsymbol{K}} \boldsymbol{a_j^H\, g_k x_k} + \boldsymbol{a_j^H n} \end{aligned} \tag{6}$$

where, $\boldsymbol{g_j}$ and $\boldsymbol{a_j}$ present the $\boldsymbol{j_{th}}$ columns of the matrixes *G* and *A*, respectively. In (6), the first term represents the $\boldsymbol{j_{th}}$ user's the desired signal, while the other two terms reflect interference from other users and noise, respectively. To put it another way, a user's desired signal is distinct from interference and noise from other users. For simplicity r the noise spectral density at unit power is considered. Therefore, the SINR is represented by Eqn. (7).

$$\boldsymbol{SINR_j} = \frac{\boldsymbol{P_t}\left|\boldsymbol{a_j^H g_j}\right|^{\boldsymbol{2}}}{\boldsymbol{P_t}\sum_{\boldsymbol{k=1, k\neq j}}^{\boldsymbol{K}}\left|\boldsymbol{a_j^H g_j}\right|^{\boldsymbol{2}} + \left\|\boldsymbol{a_j}\right\|^{\boldsymbol{2}}} \tag{7}$$

Where ‖.‖ means vector's 2-norm, and |.| indicates vector's absolute value.

4.3 Rayleigh Fading Distribution

In a complex disintegrating situation, the magnitude (*R*) of the complex envelope of the received signal follows a Rayleigh distribution if no line-of-sight path exists between the transmitter and the receiver. Eqn. (8) can be used to express the Rayleigh PDF.

$$\boldsymbol{P_r(r)} = \frac{\boldsymbol{2r}}{\boldsymbol{\Omega_p}}\exp\left(-\frac{\boldsymbol{r^2}}{\boldsymbol{\Omega_p}}\right), \qquad \boldsymbol{r \geq 0} \tag{8}$$

In this case, $\boldsymbol{\Omega_p}$ represents the average power of the envelope. It can be expressed in terms of channel coefficients as $R = |hik|$.

Receiving signals like squared envelope, which are exactly proportional to the received power, are of great importance in wireless communications because the received SNR is referred to as the received SNR. When it is multiplied by itself, a Rayleigh random variable (RV) is an exponential RV. The PDF presented in Eqn. (9) shows that the squared envelope (R2) represents an exponential distribution.

$$\boldsymbol{P_{R^2}} = \frac{\boldsymbol{1}}{\boldsymbol{\Omega_p}}\exp\left(-\frac{\boldsymbol{r}}{\boldsymbol{\Omega_p}}\right), \qquad \boldsymbol{r \geq 0} \tag{9}$$

Keeping the average envelope power constant is necessary for the purpose of simulating it. Therefore, we assume that $\Omega p = 1$. As a result, the squared envelope distribution can be represented as $|h_{ik}|^2 \sim Exp$ (1).

4.4 Distribution of Lognormal Shadowing

Given that wireless communications suffer from shadowing, applying a lognormal RV is necessary to build the received squared envelope based on practical measurements. The PDF of the lognormal distribution is shown in Eqn. (10).

$$\boldsymbol{P_v(v) = \frac{\xi}{v\sigma_{dB}\sqrt{2\pi}} \exp\left(-\frac{(\xi \log_e{}^{v} - \mu_{dB})^2}{2\sigma_{dB}}\right)} \tag{10}$$

The shadow standard deviation is given by $\boldsymbol{\sigma_{(dB)}}$, where $\xi = 10/\log_e 10$ is a scaling constant. As seen in Eqn. (10) as $V = 10^{0.1X}$, the lognormal RV is X~($\mu_{(dB)}$, $\boldsymbol{\sigma^2_{(dB)}}$). As a general rule, the $\boldsymbol{\sigma_{(dB)}}$ value lies between 4 and 12 dB. As the value of $\boldsymbol{\sigma_{(dB)}}$ increases, shadowing becomes more essential.

5. Receiver Design Analysis

The MRC receiver for a massive MU-MIMO system in a composite-fading environment is discussed in this section. We utilize (7) concerning an MRC receiver to study the SINR.

5.1 Analysis of MRC Receiver

$A = G$ is defined for M × K linear detector A of an MRC receiver when correct CSI is present; therefore $\boldsymbol{a_j} = \boldsymbol{g_j}$. Using (3) and (7), we can get the user's SINR in Eqn. (11)..

$$\begin{aligned} \boldsymbol{SINR_j^{mrc}} &= \frac{\boldsymbol{P_t \|h_j\|^4 v_j^2}}{\boldsymbol{P_t v_j \sum_{k=1,k\neq j}^{K} |h_j^H h_k|^2 v_k + \|h_j\|^2 v_j}} \\ &\triangleq \frac{\boldsymbol{P_t \|h_j\|^2 v_j^2}}{\boldsymbol{P_t v_j \sum_{k=1,k\neq j}^{K} \frac{|h_j^H h_k|^2}{\|h_j\|^2} v_k + 1}} \end{aligned} \tag{11}$$

Conditioned on $\boldsymbol{h_j}$, we represent a new RV, $\boldsymbol{g_k}$, such that $\boldsymbol{g_k} = \frac{|h_j^H h_k|}{\|h_j\|}$. A Gaussian RV with zero mean and constant variance, $\boldsymbol{g_k}$, is separated from $\boldsymbol{h_j}$; therefore, $\boldsymbol{g_k} \sim CN(0,1)$. Then, the SINR is determined in Eqn. (12) from Eqn. (6).

$$\boldsymbol{SINR_j^{mrc} = \frac{P_t \|h_j\|^2 v_j^2}{P_t v_j \sum_{k=1,k\neq j}^{K} |g_k|^2 v_k + 1}} \tag{12}$$

The BS in Eqn. (13) exhibits a single consumer, and the SNR is in the numerator, Z.

$$Z = \boldsymbol{P_t} v \sum^{M} |h_i|^2 \coloneqq \boldsymbol{P_t} v\, \gamma \tag{13}$$

The number of exponentially distributed exponential RVs with individually and identically distributed, along with a unit mean, is accounted for by $\gamma \sim \Gamma(M, 1)$.

Using Eqn. (14), the PDF of a gamma RV is stated in terms of the gamma-lognormal product distribution.

$$P_g(\gamma) = \frac{\gamma^{M-1}\exp(-\gamma)}{\tau(M)} \tag{14}$$

Where Γ(M) = (M − 1)!, since M is an integer. The distribution of a product RV, Z=VG, is given presented in Eqn. (15). In this case, Γ(M) = (M − 1)! because M is an integer. Presented in Eqn. (15) is a distribution of a product RV; therefore, Z=VG.

$$P_Z(Z) = \int_{-\infty}^{\infty} P_v(v) P_G\left(\frac{z}{v}\right)\frac{1}{|v|}dv \tag{15}$$

We tend to neglect P_i in the PDF calculation of the gamma-lognormal product since it may be a constant. The product of gamma and lognormal RV's PDF is given by the following expression from Eqn. (15):

$$P_Z(z) = \frac{{\xi_Z}^{M-1}}{(M-1)!\sigma_{(dB)}\sqrt{2\pi}}\int_0^{\infty}\frac{exp(-z/v)}{v^{(M-1)}}exp\left(\frac{-\xi\left(\log_e v-\mu_{(dB)}{}^2\right)}{2\sigma_{(dB)}^2}\right)dv \tag{16}$$

From Eqn. (16), it is evident that SNR's PDF is not locked.

5.2 Signal Detector Based on CDM

At the same time, the other variables in CDM are kept constant at their most recent updates. Cyclically, the optimization coordinate was selected. When the subproblems can be resolved frequently, the CDM is systematic.

Eqn. (17) gives the following expression for $x\mu = A\mu e^{j\theta}\mu$ in order to minimize $- Hx\|^2$ for the given equation $X-\mu \triangleq [x1, \ldots, x\mu-1, x\mu+1, \ldots, xU]$.

$$A_\mu^* = \frac{|\xi_\mu|}{\sum_{b=1}^{B}|H_{b\mu}|^2}$$

$$\theta_\mu^* = arg\{\xi_\mu\} \tag{17}$$

$$\xi_\mu \triangleq \sum_{b=1}^{B} H_{b\mu}^*\left(y_b - \sum_{v=1,v\neq\mu}^{U} H_{b\mu}A_v e^{j\theta_v}\right) \tag{18}$$

As illustrated in Eqn. (19), the optimal updating issue can be expressed in terms of equations. Using the following equation, the constant values, which do not rely on either Aμ or θμ, can be eliminated for expansion.

$$\begin{aligned} A_\mu^* e^{j\theta_\mu^*} &= \arg min\|y - H_X\|^2 \\ &= \arg\min\left|y_b - \sum_{v=1,v\neq\mu}^{U} H_{b\mu}A_v e^{j\theta_v}\right|^2 \end{aligned} \tag{19}$$

6. Simulation Results and Performance Analysis

Monte Carlo simulations are used to estimate the CDM-based detector. The simulation parameter is listed in Table 3. Gaussian random variables, (i.e., $H_{b\mu} \sim \mathcal{N}_{\mathbb{C}}(0,1/B)$, each contain an independent circularly symmetric complex in the channel matrix. The *Eb* is the bit of energy, where SNR is *Eb/N*0. Comparing things, for massive MU-MIMO systems, other approximate data detection methods were also tried, keeping the AMP detector [21], the RM detector [3], and the conventional LMMSE detector.

Table 3: Summary of the Simulated Model Parameters

Parameter	**Value**
Number of realizations in the Monte-Carlo simulations	1
Iteration	T=1, T=5
Spatial Correlation Coefficients	$\rho = 0, \rho = 0.3$
Transmit Power	*P = 0:1:20*
Total Training Power	10.^(P/10)
System Configurations (Base station × User)	128×32, 128×48
Antenna Configuration (Nt×Nr)	8×8
Constellation Modulation	QPSK, 16-QAM, 64-QAM
Signal Detection Scheme	Richardson Method, AMP, LMMSE, and CDM
SNR	0 to 20 dB/ -4 to 16 dB
Channel	MIMO
Normalization Factor	Nt*Nr

For QPSK modulation, the BER findings for antenna arrangements B × U = 128 × 32 and B × U = 128 × 48 are shown in Figures 2(a) and 2(b). Two types of time durations or slots, T = 1 and T = 5, are considered for the four techniques RM, AMP, LMMSE, and CDM. To increase the BER output of these methods, the user slides for an assigned Base station, as indicated in the figures, for the same SNR value. The BER output of the RM aided detector, the suggested CDM-based detector, and the AMP detector improve steadily as the number of repetitions increases. Except for the first two iterations, the number of iterations is similar. Still, the AMP-assisted detector works through an antenna array, and the BER result of the recommended CDM detector is higher than that of the RM detector. Compared to RM and AMP detectors, the proposed CDM-based detector requires far fewer iterations to generate the same BER output. The BER performance of the AMP detector with T = 5 is lower than that of the proposed scheme [Fig. 2(a)], and the BER performance of the referred scheme's RM detector with T = 4 is lower than that of the proposed scheme [Fig. 3(b)]. Like the proposed scheme's BER performance, the AMP with $T = 5$ is lower than the $T = 3$ [Fig. 2(a)]; the referred scheme's BER performance, the RM with $T = 4$, is lower than the $T = 3$ [Fig. 2(b)]. The proposed CDM system demonstrates a faster convergence rate.

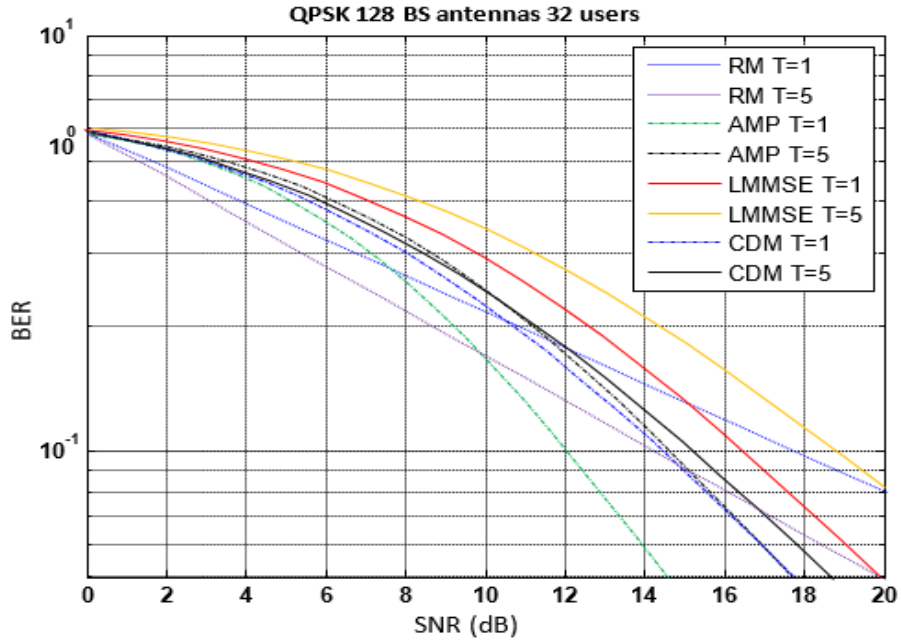

(a)

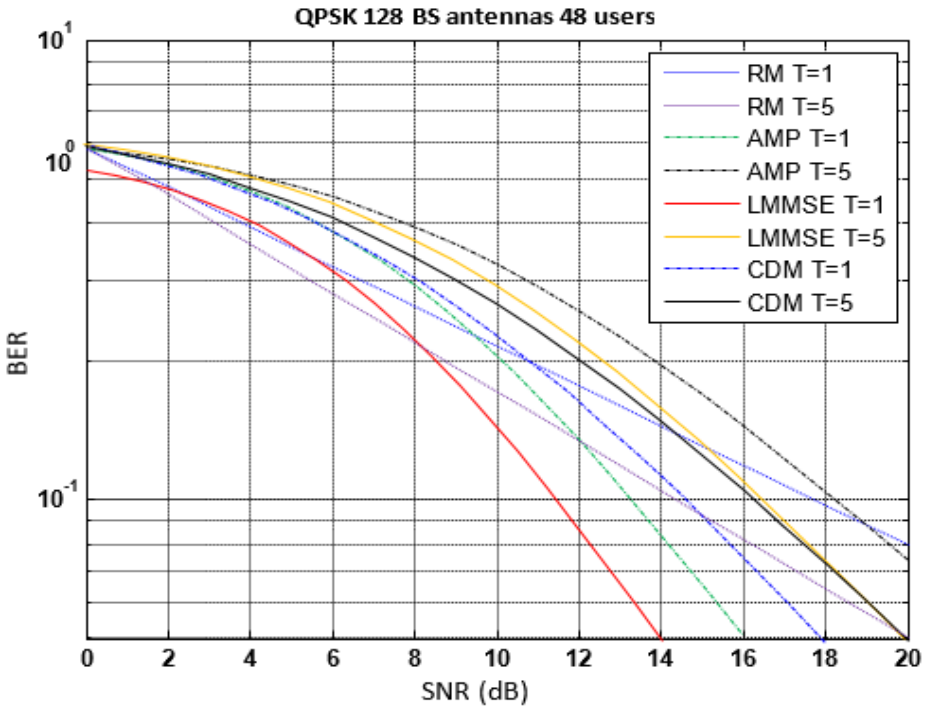

(b)Figure 2: BER antenna configuration performance for QPSK modulation with 128 × 32 (a) and QPSK modulation with 128 × 48 (b)

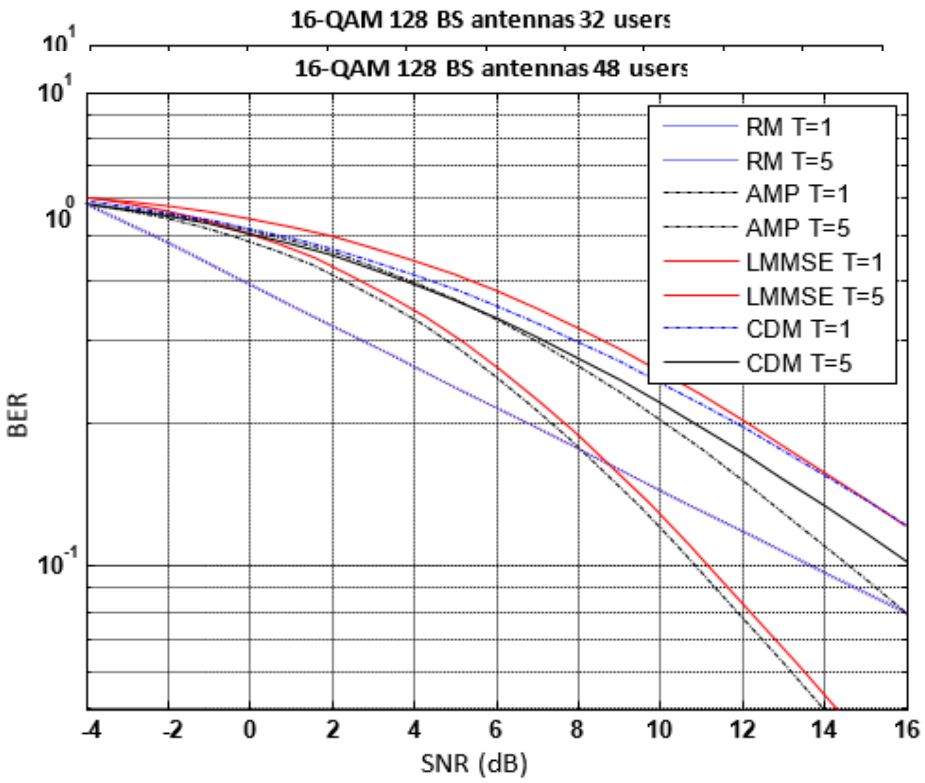

(a)

(b)

Figure 3: BER antenna configuration performance for 16-QAM modulation with 128 × 32 (a) and 16-QAM modulation with 128 × 48 (b)

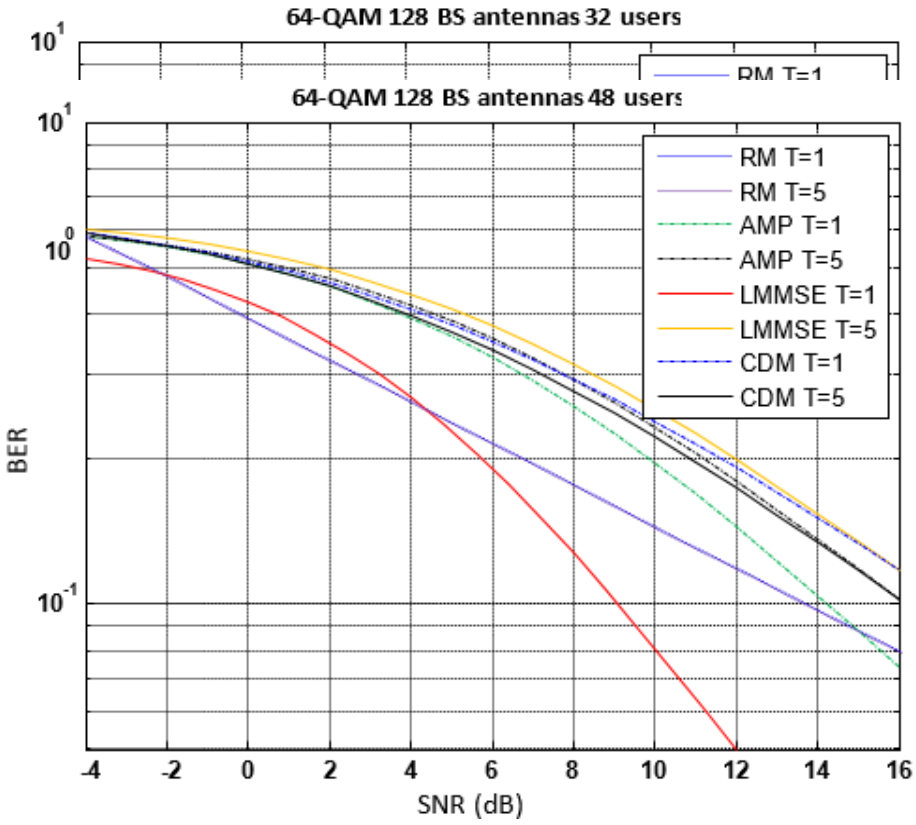

(a)

(b)

Figure 4: BER performance for 64-QAM modulation with 128 × 32 (a) and 64-QAM modulation with 128 × 48 (b)

Then, we saw the address of non-constant amplitude modulations and the proposed CDM-based transcendent detector. With 16-QAM and 64-QAM modulation, multiple antennas may be ordered. Figures 3 and 4 display the BER as an SNR feature. But for the modulation scheme, the role was similar to that in Fig. 1. Figs. 2 and 3 had almost the same output swing as seen in Fig. 2. As a result, Fig. 2 shows the BER regarding SNR where 16, and 64-QAM techniques were applied. It is evident that when the SNR increases, the impact on BER, is reduced.

When modulation order increases, the RM, AMP, and suggested CDM-based detectors require additional iterations. The optimal effects are like those shown in Fig. 2, Fig. 3, and Fig. 4. From Fig.5 below, we can observe the error in comparing the correlated channel. We achieved simulation findings for MIMO channels with identically distributed frequency-flat Rayleigh fading. Then, in radio atmospheres, the presentation of MIMO schemes is purely based on spatial correlation. As a result, the effect of channel correlation on the output of trial algorithms is being explored. The spatially correlated channel was defined as

$$H_{sc} = \sqrt{RH} \qquad (\mathbf{20})$$

Whereas, the BS correlation matrix is referred to as $R \in \mathbb{R}^{B\times B}$ [22].

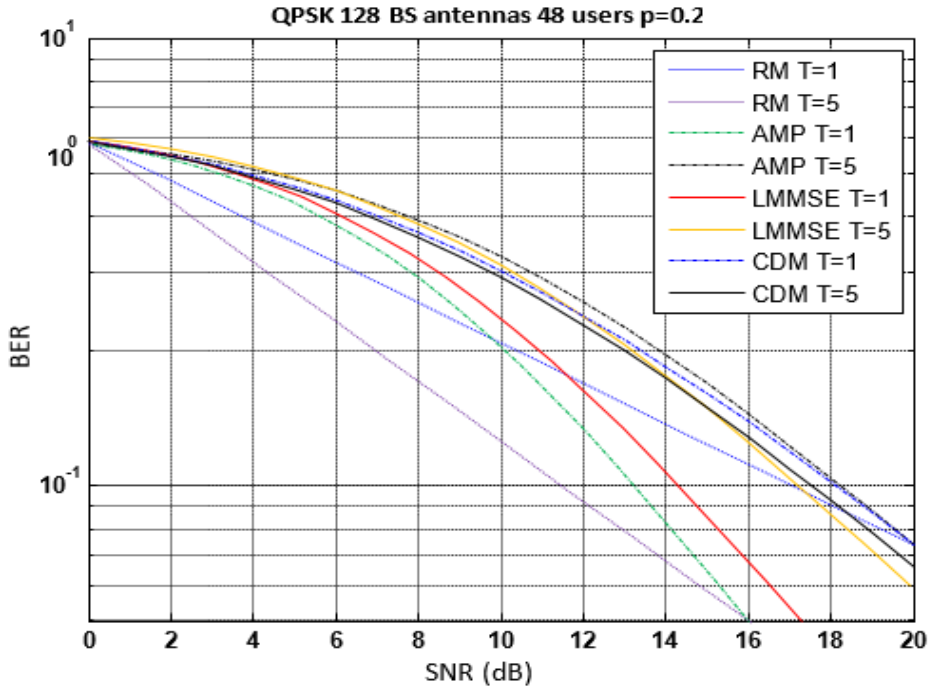

Figure 5: BER performance for QPSK modulation with 128 × 48 antenna configuration with $\rho = 0.2$

Figure 5 shows the BER results for a 128 × 48 correlated MIMO channel in the SNR example with a QPSK modulation scheme with a spatial correlation coefficient $\rho = 0.2$. Accumulative the channel correlation ρ causes little performance abasement for the LMMSE algorithm. While the suggested CDM-based detector's QPSK BER efficiency is greater than that of the LMMSE detector, the proposed CDM-based method requires a considerable number of iterations to reach convergence. Compared to the LMMSE and RM-based algorithms, the CDM-based approach is a lot simpler.

CDM-based detection is superior to machine learning (ML) detection, and this is an important finding. It is for this reason that compares the BER outcomes of the proposed CDM-based approach to those obtained using a sphere decoding (SD) technique to identify ML [23]. As reported in [24], the average computational complexity of the conservative SD algorithms and the worst case still grow exponentially with U. To use the device mentioned above parameters, the computational complexity is needed to execute SD and is challenging to achieve. For "appropriate" system configurations, we can only rationally execute SD. For [3] and [25], the simulation in this part uses a system with B × U = 128 × 16 configuration. Figures 6–8 represent the BER performances of LMMSE, CDM, and SD using 16QPSK, 16QAM, and 64-QAM modulation. The performance of ρ = 0 and ρ < 0.3 are seen in Figures 5–7 for LMMSE, CDM, and SD using different modulation techniques.

THE Figs for LMMSE, CDM, and SD utilizing QPSK, 16-QAM, and 64-QAM modulation 6–8 represent the BER performances. The BER performances of $\rho = 0$ and $\rho = 0.3$ are seen in Figures 6–8 for LMMSE, CDM, and SD using QPSK, 16-QAM, and 64-QAM modulation.

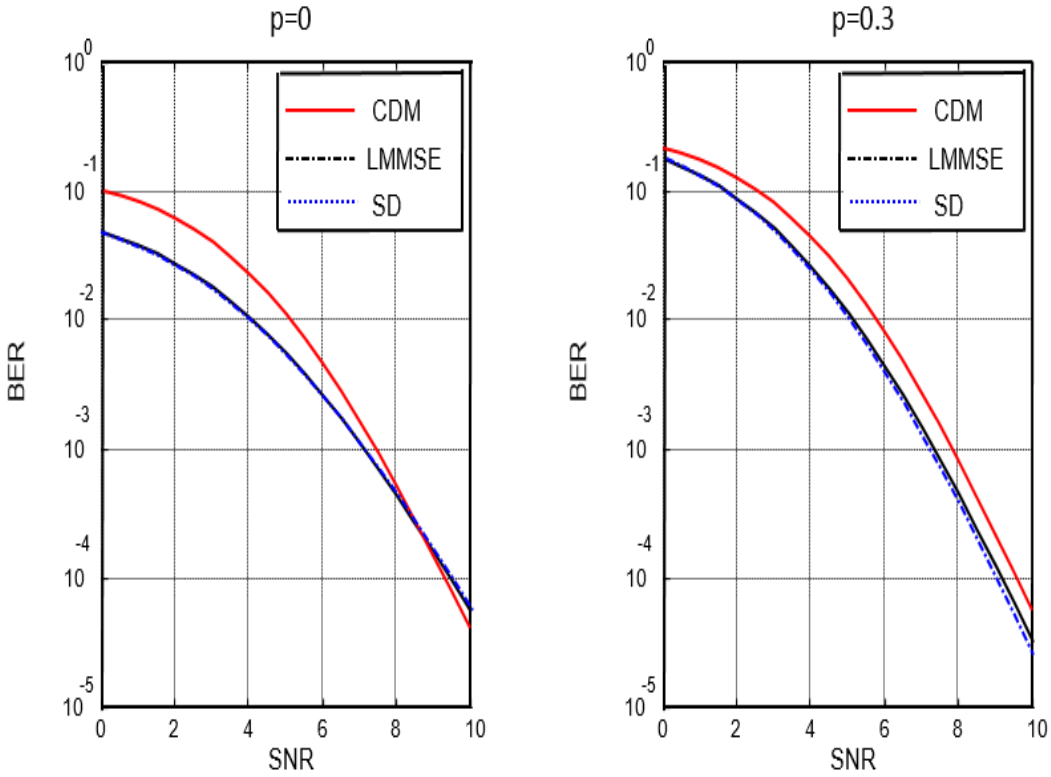

Figure 6: For 16-QPSK modulation with 128 × 16 antennas, BER performance with (a) ρ = 0 and (b) ρ = 0.3

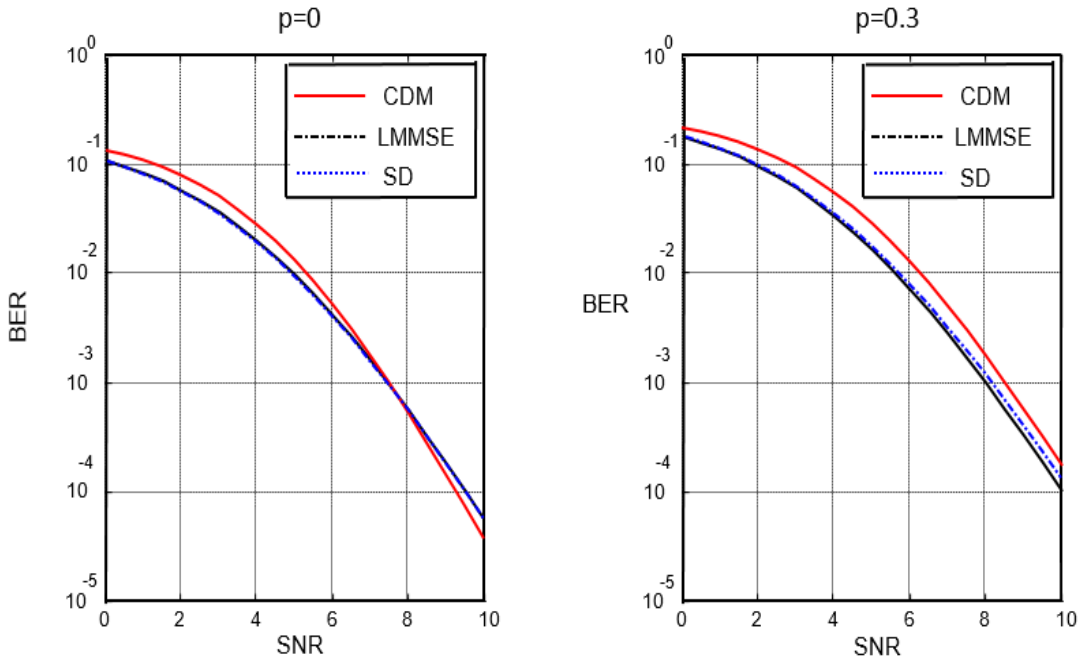

For 16-QAM modulation with 128 × 16 antennas, BER performance with (a) ρ = 0 and (b) ρ = 0.3

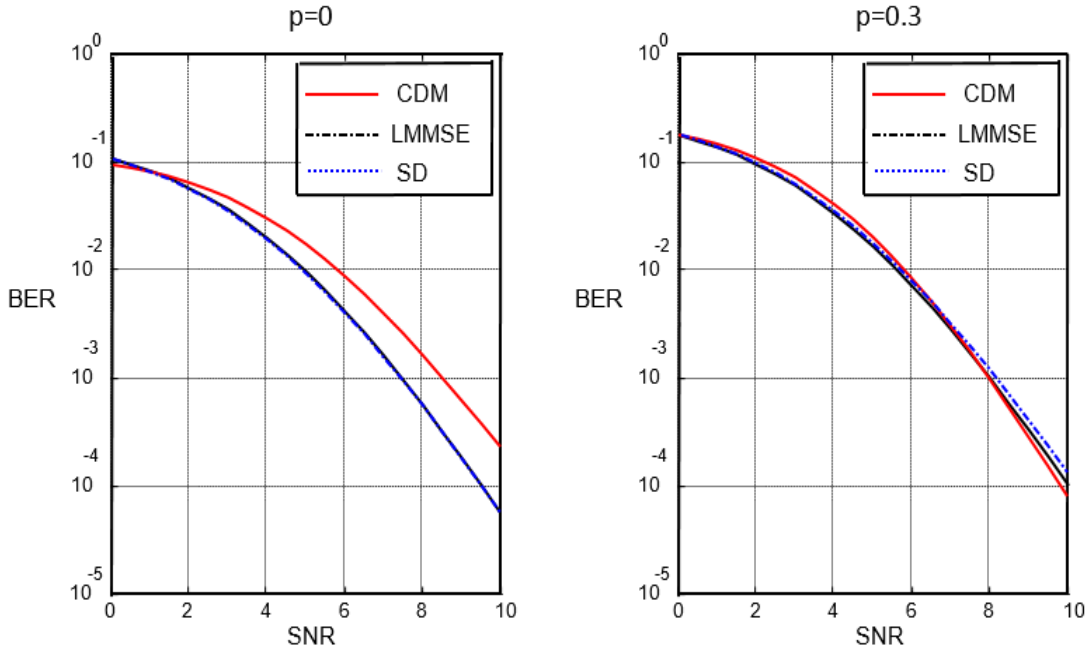

Figure 8: For 64-QAM modulation with 128 × 16 antennas, BER performance with (a) ρ = 0 and (b) ρ = 0.3

These consequences give better BER results than the traditional LMMSE algorithm or the same proposed algorithm. It is clear that the suggested CDM-based detector only accepts when contrasted to a tiny performance reduction.

In Fig.9, the impact of noise variance deprived of spatial correlation utilizing 16-QAM modulation exhibits the CDM-based detector's antenna configuration B × U = 128 × 32 massive MIMO system. From Fig.9, at 4dB, RM (T = 5) and LMMSE (T = 1) provide a better result, approximately 0.5. Conversely, LMMSE (T = 1) provides a worst result than other detectors. Finally, we can say that the other data detection techniques do not influence the proposed detector's BER performance.

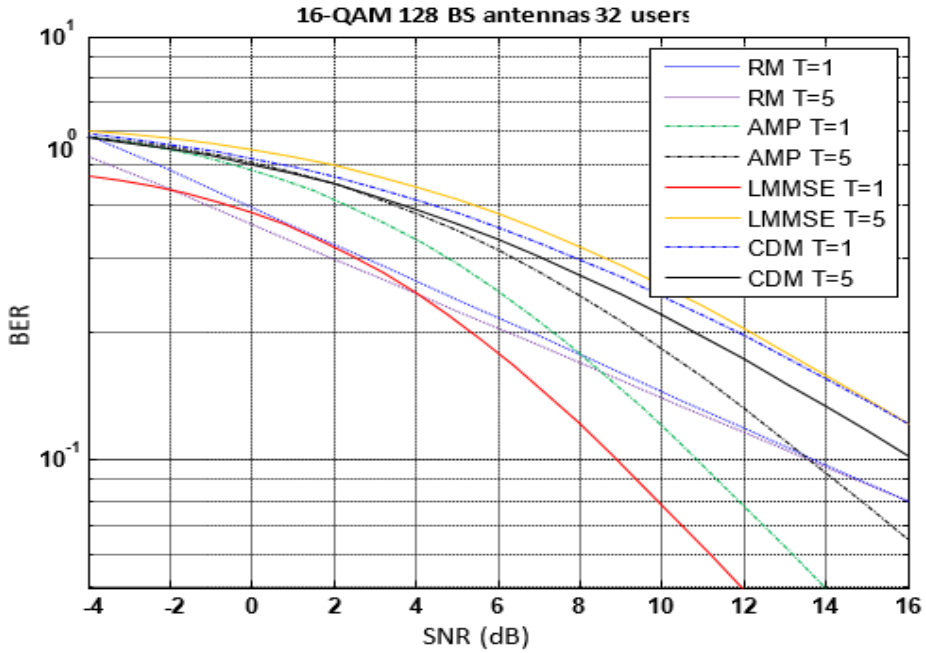

Figure 9: BER results for the 16-QAM modulation with 128 × 32 antenna configuration, where RM, AMP, LMMSE, and CDM helped the detectors take an inappropriate σ^2 from a uniform distribution.

Lastly, in Fig. 10, we saw different data detection methods for the Total Training Power concerning MSE. We can use an MRC receiver, the MSE parameter concerning the total training power. From Fig. 10, except RM detector, the other detector MSE values are approximately 1 at 0 dB. At 10 dB, the MSE value of RM detector is 1. Finally, at 20 dB, CDM provides the lowest MSE than other detectors.

Figure 10: Total Training Power versus MSE for a massive MIMO system compared to different methods RM, AMP, LMMSE, and CDM

MRC helps the CDM technique combine the proposed system resulting in better MSE performance than the other methods. This shows the efficiency of the proposed method and its effectiveness. Even though LMMSE has been around for decades, the CDM-based strategy achieved the same or superior BER performance. To put it another way, we can see that the CDM-based detector exhibits a minor performance loss compared to the SD-based detector.

7. Conclusions

This paper proposes an energy-efficient and low-complexity data detection process for uplink massive MU-MIMO systems. The optimal and suboptimal data detection algorithms like LMMSE and approximate message passing may not provide a satisfactory BER performance. The existing low-complexity AMP algorithm will converge incorrectly when the MIMO channels are spatially correlated. Here, MRC receiver is considered for a very large-scale MU-MIMO system in a composite-fading condition combined with the CDM technique. The CDM is considered because of its low complexity and better performance than other conventional techniques. The simulation results show that the proposed system outputs better MSE or BER performance. The comparison results analyzing total training power concerning MSE for the different RM, AMP, LMMSE, and CDM show the proposed system's energy efficiency. Thus, this new approach is substantially energy efficient and less complicated. For future recommendations, this work can be extended to a multi-cell situation. Massive MIMO detectors' accuracy bounds in spatially correlated channels are unknown. Next, a rigorous investigation is required to quantify the performance bounds used as a benchmark instead of the maximum likelihood detector, whose performance cannot be simulated for Massive MIMO systems. The complexity of the algorithm's execution time needs to reduce by using potential parallelization. It covered a wide range of studies on the fundamental theory on the CSMA/CA, IEEE 802.15.4, ISA 100.11a, and literature review and presented energy-efficient GMAC protocol methodology.

Acknowledgments: This work has been supported by the Universiti Kebangsaan Malaysia (UKM) under GGPM 2020-028.

Conflicts of Interest: "The authors declare no conflict of interest."

References

1. T. L. Marzetta, "Noncooperative cellular wireless with unlimited numbers of base station antennas." IEEE Trans. Wireless. Commun., vol. 9, no. 11, pp. 3590-3600, Nov. 2010.
2. F. Rusek, D. Persson, B. K. Lau, E. G. Larsson, T. L. Marzetta, O. Edfors, and F. Tufvesson. "Scaling up MIMO: Opportunities and challenges with very large arrays." IEEE Signal Process. Mag., vol. 30, pp. 40-60, Jan. 2013.
3. X. Gao, L. Dai, Y. Ma, and Z. Wang, "Low-complexity near-optimal signal detection for uplink large-scale MIMO systems." Electron. Lett., vol. 50, no. 18, pp. 1326–1328, Aug. 2014.
4. D. L. Donoho, A. Maleki, and A. Montanari, "Message-passing algorithms for compressed sensing." Proc. Nat. Acad. Sci. USA, vol. 106, no. 45, pp. 18914–18919, Nov. 2009.
5. W. Saad, M. Bennis, and M. Chen, "A vision of 6G wireless systems: Applications, trends, technologies, and open research problems." IEEE Network, vol. 34, no. 3, pp. 134–142, Oct. 2020.
6. J.-C. Chen, "A low complexity data detection algorithm for uplink multi-user massive MIMO systems." IEEE Journal on Selected Areas in Communications, vol. 35, no. 8, Aug. 2017.
7. M. S. Zia and S. A. Hassan, "On the impacts of composite fading on large scale multi-user MIMO systems." IEEE Communications Letters, vol.19, no. 12, Dec. 2015.
8. A. Boukharouba, M. Dehemchi, and A. Bouhafer. "Low-complexity signal detection and precoding algorithms for multi-user massive MIMO systems." SN Appl. Sci. vol. 3, pp. 169 2021. https://doi.org/10.1007/s42452-020-04085-z
9. R. M. Asif, J. Arshad, M. Shakir, S. M. Noman, A. U. Rehman, "energy efficiency augmentation in massive MIMO systems through linear precoding schemes and power consumption modeling." Wireless Communications and Mobile Computing, vol. 2020, Article ID 8839088, 13 pages, 2020. https://doi.org/10.1155/2020/8839088

10. M. K. Hasan, A. F. Ismail, S. Islam, W. Hashim, and B. Pandey. “Dynamic spectrum allocation scheme for heterogeneous network.” Wireless Personal Communications. vol. 95, no. 2, pp. 299-315, 2017.
11. M. K. Hasan, A. F. Ismail, S. Islam, W. Hashim, M. M. Ahmed, and I. Memon. “A novel HGBBDSA-CTI approach for subcarrier allocation in heterogeneous network.” Telecommunication Systems. vol. 70, no. 2, pp. 245-62, Feb. 2019.
12. H. M. Kamrul, T. C. Chuah, A. A. El-Saleh, M. Shafiq, S. A. Shaikh, S. Islam, and M. Krichen. “Constriction Factor Particle Swarm Optimization based load balancing and cell association for 5G heterogeneous networks.” Computer Communications vol. 180, pp. 328-337, 2021.
13. H. M. Kamrul, A. F. Ismail, S. Islam, W. Hashim, and B. Pandey. “Dynamic spectrum allocation scheme for heterogeneous network.” Wireless Personal Communications vol. 95, no. 2, pp. 299-315, 2017.
14. D. L. Donoho, A. Maleki, and A. Montanari, “Message-passing algorithms for compressed sensing.” Proc. Nat. Acad. Sci., vol. 106, no. 45, pp. 18 914–18 919, Nov. 2009.
15. Z. Chuan, W. Zhizhen, S. Christoph, Z. Zaichen, and X. You. (2018). “Efficient soft-output gauss-seidel data detector for massive MIMO systems.” IEEE Transactions on Circuits and Systems I: Regular Papers. PP. 10.1109/TCSI.2018.2875741.
16. X. Gao, L. Dai, Y. Ma, and Z. Wang, "Low-complexity near-optimal signal detection for uplink large-scale MIMO systems." Electron. Lett., vol. 50, no. 18, pp. 1326–1328, Aug. 2014.
17. Q. Deng, L. Guo, C. Dong, J. Lin, D. Meng, and X. Chen, “High throughput signal detection based on fast matrix inversion updates for uplink massive multiuser multiple-input multi-output systems.” IET Commun., vol. 11, no. 14, pp. 2228–2235, 2017.
18. X. Peng, W. Wu, J. Sun, and Y. Liu, “Sparsity-boosted detection for large mimo systems.” IEEE Commun. Lett., vol. 19, no. 2, pp. 191–194, Feb. 2015.
19. R. He, J. Kang, Y. Xiao and S. Fang, "Coordinate descent method for signal detection in IDMA.” 2019 IEEE 89th Vehicular Technology Conference (VTC2019-Spring), 2019, pp. 1-5, doi: 10.1109/VTCSpring.2019.8746371.
20. I. Shayla, O. O. Khalifa, A.-H. A. Hashim, M. K. Hasan, M. Razzaque, and B. Pandey. "Design and evaluation of a multihoming-based mobility management scheme to support inter technology handoff in PNEMO." Wireless Personal Communications vol. 114, no. 2, 1133–1153, 2021.
21. M. K. Hasan, I. Shayla, I. Memon., A. F. Islmail, S. Abdullah, A. K. Budati, and N. K. Nafi, “A Novel resource oriented DMA framework for internet of medical things devices in 5G network" IEEE Transactions on Industrial Informatics, 2021.
22. J. Choi, S. R. Kim, and I. K. Choi, "Statistical Eigen-beamforming with selection diversity for spatially correlated OFDM downlink.” IEEE Trans. Veh. Technol., vol. 56, no. 5, pp. 2931– 2940, Sep. 2007.
23. A. Burg, M. Borgmann, M. Wenk, M. Zellweger, W. Fichtner, and H. Bolcskei, "VLSI implementation of MIMO detection using the sphere decoding algorithm.” IEEE J. Solid-State Circuits, vol. 40, no. 7, pp. 1566–1577, Jul. 2005.
24. D. Seethaler, J. Jaldén, C. Studer, and H. Bölcskei, "On the complexity distribution of sphere decoding.” IEEE Trans. Inf. Theory, vol. 57, no. 9, pp. 5754–5768, Sep. 2011.
25. L. Dai, X. Gao, X. Su, S. Han, C.-L. I, and Z. Wang, "Low-complexity soft-output signal detection based on Gauss-Seidel method for uplink multi-user large-scale MIMO systems.” IEEE Trans. Veh. Technol., vol. 64, no. 10, pp. 4839–4845, Oct. 2015.